

Andreev tunneling and Josephson current in light irradiated graphene

Debabrata Sinha and Satyaki Kar*

Theoretical Physics Department, Indian Association for the Cultivation of Science, Jadavpur, Kolkata-700032, India.

(Dated: June 21, 2018)

We investigate the Andreev tunneling and Josephson current in graphene irradiated with high-frequency linearly polarized light. The corresponding stroboscopic dynamics can be solved using Floquet mechanism which results in an effective stationary theory to the problem exhibiting an anisotropic Dirac spectrum and modified pseudospin-momentum locking. When applied to an irradiated normal graphene - superconductor (NS) interface, such analysis reveal Andreev reflection (AR) to become an oscillatory function of the optical strength. Specifically we find that, by varying the polarization direction we can both suppress AR considerably or cause the Andreev transport to remain maximum at sub-gap excitation energies even in the presence of Fermi level mismatch. Furthermore, we study the optical effect on the Andreev bound states (ABS) within a short normal-graphene sheet, sandwiched between two *s*-wave superconductors. It shows redistribution of the low energy regime in the ABS spectrum, which in turn, has major effect in shaping the Josephson super-current. Subjected to efficient tuning, such current can be sufficiently altered even at the charge neutrality point. Our observations provide useful feedback in regulating the quantum transport in Dirac-like systems, achieved via controlled off-resonant optical irradiation on them.

PACS numbers:

I. INTRODUCTION

The quantum transport in graphene^{1,2}, with its low energy Dirac spectrum¹⁻⁴ at the edges of the Brillouin zone, has remained an engaging field of study ever since its inception in 2004⁵. Though experimental difficulties still remain in detecting its transport characteristics at the edges⁶, its bulk behavior, described by the massless, chiral fermions⁴ has been quite well probed by now. Tuning such system with straining or introducing gap in the Dirac spectrum witness noticeable variations in the charge transport. Particularly, graphene based superconductor—normal—superconductor (SNS) junction can be tuned to enhance supercurrent at the charge neutrality point upon straining⁷ or an energy gap can enhance the pseudospin inverted Andreev conductance in a graphene-based superconductor/pseudoferrromagnet junction⁸. As it turns out, such modifications can be easily implemented via optical irradiation. The transport properties of the Dirac-like systems are very much susceptible to light irradiation and produce interesting outcomes such as exciting surface plasmon polaritons⁹⁻¹¹ in graphene sheet, enhancing controllability of electrostatics in graphene-based metamaterials^{12,13} or allowing photo-reduction of graphene-oxide films to tune wettability¹⁴ and so on.

The energetics of the charge carriers of a graphene monolayer, periodically driven via high frequency electromagnetic light waves with electrons strongly coupled to the photons, has been analyzed recently¹⁵⁻²¹ using Floquet theory. There, the electrons get dressed by the field exhibiting drastic changes in the dispersion. For example, it is observed that the circularly polarized light create a field induced gap at the charge neutrality or Dirac point²²⁻²⁴. In contrast the energy spectrum of electrons dressed by linearly polarized light is modified by

Bessel function and it remains gapless. The physical properties of dressed electrons have been studied in various condensed matter systems including quantum well²⁵⁻²⁷, quantum rings²⁸ and in recently in Dirac materials like graphene^{16,24,31}, Weyl semimetals²⁹ and topological insulators³⁰. In graphene related systems, particularly attentions paid to the transport properties of dressed electrons in *p* – *n* junctions³¹, magnetotransport¹⁵ and spin transport of dressed electrons¹⁷, optical response of dressed electrons¹⁹ and field induced topological phase transition³¹⁻³³.

Though an effective stationary theory is constructed for stroboscopic evolution of the fermionic wavefunction under light irradiation, to the best of our knowledge, no study on transport behavior of the light irradiated superconducting graphene junctions has been performed yet. We would like to bridge this gap in the literature and study the tunneling conductance of a normal metal-superconductor (NS) junction as well as the Andreev bound state (ABS) and Josephson current of a SNS junction in a strongly irradiated graphene sheet. As a primary investigation, this paper deals with only irradiation via linearly polarized light. A graphene is a semimetal in which superconductivity can be induced via proximity effect³⁴. Transport through a NS junction experiences Andreev reflection (AR) for energy-bias smaller than the superconducting gap³⁵. The resulting electron-hole conversion in the Normal (N) sub-system and the Cooper pair production in the superconductor (S) counterpart develops a finite conductance across the NS junction. An irradiation via linearly polarized light offers a tuning parameter α (which is a function of both intensity and frequency of the light, to be elaborated later on) to the problem. In the off-resonant conditions, the quasi-particle velocities along a direction normal to the irradiated field get reduced, from its original graphene Fermi velocity v_F , by a factor of Bessel's function $J_0(\alpha)$. Thus the low energy spectrum of graphene becomes anisotropic, tunable by the optical parameter α . This tunability allows for considerable variation in the Andreev current and subgap conductance

*Corresponding author:satyaki.phys@gmail.com

becomes an oscillatory function in α . With rotation of the plane of polarization, this current can be enhanced to maximum or suppressed considerably, as can be found from our calculation and results in section III.

In this work we also study the Andreev bound states (ABS) and Josephson current on a light irradiated SNS junction in graphene. The analysis of ABS and Josephson current in graphene SNS junction is well studied in the literature^{36–38}. Our objective is to probe the effect of linearly polarized light on such system/assembly. We find that the low energy spectrum of the ABS get sufficiently affected by the optical irradiation. As a result, the Josephson current get enhanced or suppressed depending on the direction of polarization as well as the value of the chemical potential. Signature of such modifications are found at the charge neutrality point as well, even though the density of state vanishes there. These interesting observations, in fact, can provide possible route to control quantum transport in graphene with relevance to the spintronic based applications.

We reiterate here that the Hamiltonian of our light irradiated system is time periodic due to the presence of a time dependent field of polarization and we resort to the Floquet formalism to analyze the stroboscopic dynamics^{20,39} of this time-periodic problem. Recently several authors have used the Floquet theory in the context of Dirac materials^{15–17,30,33}. It generally presumes the frequency of the optical field to be off-resonant and thus does not cause any direct electronic transition³¹. This can be achieved if the photon energy of the polarized light meets the condition $\omega\tau_0 \gg 1$ where τ_0 is the relaxation time of the unirradiated graphene¹⁶. In the off-resonant condition, energy conservation can thus be respected within a first order perturbation theory resulting in an effective stationary Hamiltonian of the problem. Our construction, in presence of a linearly polarized light, closely follows the work presented in Ref.17.

The rest of the paper is organized as follows. In section II, we describe the Floquet theory to derive the stationary Hamiltonian that we later work on. In section III we describe the Andreev transport in irradiated graphene NS junction. In section IV, we describe ABS and Josephson current through the corresponding SNS junction and finally in section V, we summarize our work and conclude.

II. EFFECTIVE STATIONARY THEORY

As mentioned in the Introduction, what follows below for the derivation of the stationary Hamiltonian of our irradiated problem is an simple extension of the work performed in Ref.15–18.

The low energy physics in graphene, around the Dirac point, are described by the linear Hamiltonian $H_{\mathbf{k}} = \hbar v_F \sigma \cdot \mathbf{k}$ where σ & \mathbf{k} denote the pseudo-spin (originating from the two sublattice indices in the underlying honeycomb lattice) and the wave-vectors of the Dirac particles respectively. In presence of a polarizing field, the canonical momentum gets the Pierel's substitution yielding $H_{\mathbf{k}} = \hbar v_F \sigma \cdot (\mathbf{k} + e\mathbf{A})$, where \mathbf{A} denotes the magnetic vector potential. Electrons/holes get

dressed by the field¹⁵ and those quasiparticles, for an electric field $E = E_0 \sin(\omega t) [\cos \theta_0 \hat{x} + \sin \theta_0 \hat{y}]$, are described by the Hamiltonian

$$H_{\mathbf{k}} = \hbar v_F [\sigma_x k_x + \sigma_y k_y] + \frac{ev_F E_0 \cos(\omega t)}{\omega} [\cos \theta_0 \sigma_x + \sin \theta_0 \sigma_y], \quad (1)$$

with the Schrödinger equation given by, $i\dot{\psi}_{\mathbf{k}} = H_{\mathbf{k}}\psi_{\mathbf{k}}$.

In the basis of spinor $s_+ = (1 \ 0)^T$ and $s_- = (0 \ 1)^T$, we have $\sigma_z s_{\pm} = \pm s_{\pm}$. At the Dirac point, the wavefunction $\psi_{\mathbf{k}=0}$ actually corresponds to the non-stationary part $H_0 = \frac{ev_F E_0 \cos(\omega t)}{\omega} [\cos \theta_0 \sigma_x + \sin \theta_0 \sigma_y]$, which appears due to the presence of the electromagnetic field. Its eigenstates, compatible with the Schrodinger equation, are given by

$$\psi_0^{\pm} = \frac{1}{\sqrt{2}} [e^{-i\theta_0} s_+ \pm s_-] e^{\mp i(\alpha/2) \sin(\omega t)}, \text{ where } \alpha = \frac{2ev_F E_0}{\hbar\omega^2}$$

and they represent the time-dependent basis for the problem. So the general wave-function can be written as,

$$\psi_{\mathbf{k}} = a_{\mathbf{k}}^+(t) \psi_0^+ + a_{\mathbf{k}}^-(t) \psi_0^- \quad (= c_+(t) s_+ + c_-(t) s_-) \quad (2)$$

where the coefficients of the two basis are related as

$$\begin{pmatrix} c_+(t) \\ c_-(t) \end{pmatrix} = \begin{pmatrix} e^{-i\theta_0} \\ 1 \end{pmatrix} [a_{\mathbf{k}}^+(t) e^{-i\frac{\alpha}{2} \sin(\omega t)} \pm a_{\mathbf{k}}^-(t) e^{i\frac{\alpha}{2} \sin(\omega t)}].$$

Solution to the Schrodinger equation, in the time-dependent basis then gives $i\hbar\partial\psi_{\mathbf{k}}/\partial t = H_{\mathbf{k}}\psi_{\mathbf{k}}$ i.e.,

$$i\dot{a}_{\mathbf{k}}^{\pm}(t) = \pm v_F \{ \{ k_x a_{\mathbf{k}}^{\pm}(t) + i k_y e^{\pm i\alpha \sin(\omega t)} a_{\mathbf{k}}^{\mp}(t) \} \cos \theta_0 + \{ k_y a_{\mathbf{k}}^{\pm}(t) - i k_x e^{\pm i\alpha \sin(\omega t)} a_{\mathbf{k}}^{\mp}(t) \} \sin \theta_0 \}. \quad (3)$$

Let us now bring in the Floquet picture for this periodically driven system, which says that for stroboscopic evolution we can write $\psi_{\mathbf{k}}(t+T) = e^{-i\epsilon_{\mathbf{k}} T} \psi_{\mathbf{k}}(t)$, $T = 2\pi/\omega$ being the time period of the field. Here $\epsilon_{\mathbf{k}}$ is the quasi-energy of the Floquet mode which turns out to be the eigenvalue of the corresponding Floquet Hamiltonian. We can absorb this exponential dependence in the coefficients $a_{\mathbf{k}}^{\pm}$ and write a frequency-Fourier transform as

$$a_{\mathbf{k}}^{\pm}(t) = e^{-i\epsilon_{\mathbf{k}} t} \sum_n \tilde{a}_{\mathbf{k},n}^{\pm} e^{in\omega t}.$$

With this, Eq. 3 becomes

$$(\epsilon_{\mathbf{k}} - n\omega) \tilde{a}_{\mathbf{k},n}^{\pm} = \pm v_F \{ \{ k_x \tilde{a}_{\mathbf{k},n}^{\pm} + i \sum_{n'} J_{n-n'}(\pm\alpha) k_y \tilde{a}_{\mathbf{k},n'}^{\mp} \} \cos \theta_0 + \{ k_y \tilde{a}_{\mathbf{k},n}^{\pm} - i \sum_{n'} J_{n-n'}(\pm\alpha) k_x \tilde{a}_{\mathbf{k},n'}^{\mp} \} \sin \theta_0 \} \quad (4)$$

where we utilize Jacoby-Anger formula, $e^{ix \sin(t)} = \sum_{m=-\infty}^{\infty} J_m(x) e^{imt}$ with $J_m(x)$ denoting the Bessel's function of first kind. Now we consider only the 1st Floquet zone as the Floquet replicas corresponding to $n \neq 0$ can be disre-

garded as long as ω is large enough compared to the frequencies corresponding to any direct electronic transition between the conduction electrons. Next, it is evident that at high frequency or very small E_0 (*i.e.*, small α), $J_{n'}(\alpha)$ is dominant for $n' = 0$. Also the quantum amplitude $\tilde{a}_{\mathbf{k},n'}^\pm$, for $n' \neq 0$, correspond to emission/absorption of n' photons by the electrons and hence smaller compared to the $a_{\mathbf{k},0}^\pm$. These two conditions, together, justifies the second approximation of considering only the $n' = 0$ term in Eq. 4. It basically relies on the limit

$$|J_{n'}(\alpha)a_{\mathbf{k},n'}^\pm/J_0(\alpha)a_{\mathbf{k},0}^\pm| \ll 1 \quad (5)$$

for $n' \neq 0$, as described in Ref.15–17. Hence it excludes the points where $J_0(\alpha) \rightarrow 0$ and with the large off-resonant frequency considered, no n-photon absorption or emission process remains present^{15–17} within the approximation. However, to keep our results more accountable, we consider only small values of α for drawing any conclusion from our work.

This leads us to the equation,

$$\begin{aligned} \epsilon_{\mathbf{k}}\tilde{a}_{\mathbf{k},0}^\pm &= \pm v_F[\{k_x\tilde{a}_{\mathbf{k},0}^\pm + iv_F J_0(\alpha)k_y\tilde{a}_{\mathbf{k},0}^\mp\}\cos\theta_0 \\ &+ \{k_y\tilde{a}_{\mathbf{k},0}^\pm - iv_F J_0(\alpha)k_x\tilde{a}_{\mathbf{k},0}^\mp\}\sin\theta_0]. \end{aligned} \quad (6)$$

Eq. 6 is just like a stationary Schrödinger equation with an effective Hamiltonian given by

$$\begin{aligned} H' &= \hbar[\{\sigma_z v_F k_x - \sigma_y v_F J_0(\alpha)k_y\}\cos\theta_0 \\ &+ \{\sigma_z v_F k_y + \sigma_y v_F J_0(\alpha)k_x\}\sin\theta_0] \end{aligned} \quad (7)$$

which can be unitary transformed to get a conventional form,

$$\begin{aligned} H &= \hbar v_F[\{\sigma_x k_x + \sigma_y J_0(\alpha)k_y\}\cos\theta_0 \\ &+ \{\sigma_x k_y - \sigma_y J_0(\alpha)k_x\}\sin\theta_0] \end{aligned} \quad (8)$$

So, the Hamiltonian of a graphene get modified when irradiated with a linearly polarized light. Eq.(8) shows that, the velocity vector is not parallel to the wave-vector (unless direction of propagation is along x or y) and thus quasiparticle trajectory deviates from that it would be in absence of the light irradiation. Note that, this Floquet theory formalism can be extended to a circularly polarized light as well. It is well established that, circularly polarized light introduces a gap at the Dirac point of graphene by breaking the time reversal symmetry. However, as mentioned earlier, this paper confines only in studying the effects of a linearly polarized light. In the next following section, we use the Hamiltonian Eq.(8) for our light irradiated system and discuss what consequences it leads to in the context of Andreev transport, ABS and Josephson current. To be precise, all the results that are presented in this paper, correspond to two values of θ_0 , namely $\theta_0 = 0$ and $\theta_0 = \pi/2$.

III. IRRADIATED GRAPHENE N-S JUNCTION

We consider a NS junction in an irradiated graphene sheet occupying the $x - y$ plane with normal region at $x < 0$ and superconducting region at $x > 0$. The superconductiv-

ity in graphene is induced via proximity effect when a superconducting electrode is kept close to a graphene sheet¹. Either side of the junction can be described by the Dirac-Bogoliubov-de Gennes (DBdG) equations¹

$$\begin{pmatrix} \mathcal{H}_\pm - \mu + U(r) & \Delta(r) \\ \Delta^*(r) & \mu - U(r) - \mathcal{H}_\pm \end{pmatrix} \Psi_\pm = \epsilon \Psi_\pm \quad (9)$$

Here, $\Psi_\pm = (u_\pm, v_\pm)$ is the 4-component fermionic wave function where the electron-like and hole-like spinors are given as $u_\pm = (\Psi_{A\pm}, \Psi_{B\pm})$ and $v_\pm = (\Psi_{A\pm}^*, -\Psi_{B\pm}^*)$ respectively. u_\pm and v_\mp are time-reversal partner of each other, as the Hamiltonian possess time-reversal symmetry. The index $+$ ($-$) stands for two valley K and K' points (that constitutes the Fermi surface in the undoped graphene). μ denotes the Fermi energy, A and B indicates the two sublattices within the hexagonal lattice of graphene. In graphene, electron and hole states are connected and can originate from same branch of the electronic spectrum. Moreover, the quasiparticles require two-component wavefunction description to define relative contributions of the sublattices A and B⁴⁰. This sublattice or equivalent pseudospin index give the notion of chirality in the graphene transport. The spin-singlet pair potential $\Delta(r)$ in Eq.(9) is modeled as $\Delta(r) = \Delta_0 e^{i\phi} \Theta(x)$ where Δ_0 and ϕ are the amplitude and phase of the induced superconducting order parameter, respectively. In superconducting region there is a gap in the energy spectrum $|\Delta| = \Delta_0$ at the Fermi energy. The potential $U(r)$ give the relative shift of Fermi energy between the normal and superconducting regions of graphene sheet and modelled by $U(r) = -U_0 \Theta(x)$. As we discussed, linearly polarized light does not break the valley degeneracy of graphene and for calculations, it suffices to concentrate only on a single valley.

Quantitative analysis of Andreev tunneling in a graphene NS junction has been done extensively in Ref. 1,2,41. As we find that a high frequency irradiation modifies only one component of the quasiparticle velocity, we briefly touch upon those derivations for anisotropic carrier velocities, in the following.

The energy spectrum in N or S region can be written as

$$\epsilon = \sqrt{|\Delta|^2 + [\mu - U(r) \pm (\hbar^2 v_x^2 k_x^2 + \hbar^2 v_y^2 k_y^2)^{\frac{1}{2}}]^2} \quad (10)$$

From Eq.(9), one can find the wave function in the normal and superconducting region. In the normal region, for electrons (holes) traveling in the $\pm x$ ($-x$) direction with a transverse momentum k_y and excitation energy ϵ , the wave functions are given by

$$\begin{aligned} \Psi_N^{e+} &= (1, e^{i\theta_N^e}, 0, 0)^T \exp(ik_x^e x) \\ \Psi_N^{e-} &= (1, -e^{-i\theta_N^e}, 0, 0)^T \exp(-ik_x^e x) \\ \Psi_N^{h-} &= (0, 0, 1, e^{-i\theta_N^h})^T \exp(-ik_x^h x) \end{aligned} \quad (11)$$

where $k_{x(y)}^{e(h)} = p_{x(y)}^{e(h)}/\hbar$ and we define,

$$\begin{aligned} e^{i\theta_N^e} &= \frac{v_x \cos \theta_e + i v_y \sin \theta_e}{v_0^e} \\ e^{i\theta_N^A} &= \frac{v_x \cos \theta_h + i v_y \sin \theta_h}{v_0^h} \\ v_0^{e(h)} &= \sqrt{v_x^2 \cos^2 \theta_{e(h)} + v_y^2 \sin^2 \theta_{e(h)}}. \end{aligned} \quad (12)$$

Here θ_e is the angle of incidence of the electron and θ_h is the Andreev reflected angle for a hole across the interface. Due to the anisotropy in the spectrum (*i.e.*, $v_x \neq v_y$), $\theta_N^e \neq \theta_e$, in general and thus the pseudospin-momentum locking of the unirradiated graphene gets lost here. Rather a modified α -dependent relation exists between pseudospin and \mathbf{k} directions. The critical angle for Andreev reflection (θ_c) turns out to be

$$\theta_c = \sin^{-1} \frac{\frac{|\epsilon - \mu|}{\epsilon + \mu} v_x}{\sqrt{\left(\frac{|\epsilon - \mu|}{\epsilon + \mu}\right)^2 v_x^2 + v_y^2 \left(1 - \left(\frac{|\epsilon - \mu|}{\epsilon + \mu}\right)^2\right)}}. \quad (13)$$

Note that, in a normal graphene (in absence of dressing field) $v_x = v_y = v_F$ and the value of θ_c is given in Ref.1.

In the superconducting region, the BdG equation describes the electron and hole quasiparticle mixture or Bogoliubons and opens a gap at the Fermi level. There the wave functions take the form

$$\begin{aligned} \Psi_S^+ &= (u(q_e), u(q_e)e^{i\theta_S^e}, v(q_h), v(q_h)e^{i\theta_S^e})^T \exp(iq_x^e x) \\ \Psi_S^- &= (v(q_h), -v(q_h)e^{-i\theta_S^h}, u(q_e), -u(q_e)e^{-i\theta_S^h})^T \exp(-iq_x^h x) \end{aligned} \quad (14)$$

where

$$\begin{aligned} u(q_e) &= \sqrt{\frac{1}{2} \left(1 + \frac{\sqrt{\epsilon^2 - \Delta_0^2}}{\epsilon}\right)}, v(q_h) = \sqrt{\frac{1}{2} \left(1 - \frac{\sqrt{\epsilon^2 - \Delta_0^2}}{\epsilon}\right)}, \\ e^{i\theta_S^e} &= \hbar(v_x q_x^e + i v_y k_y) / (\mu + U_0 + \Omega), \\ e^{-i\theta_S^h} &= \hbar(v_x q_x^e + i v_y k_y) / (\mu + U_0 - \Omega), \quad \Omega = \sqrt{\epsilon^2 - \Delta_0^2}. \end{aligned} \quad (15)$$

Wave-vectors q_x^e and q_x^h can be obtained from Eq.(10) in the superconducting region.

Now for an electron incident at the junction from the normal side, and with excitation energy ϵ and transverse momentum p_y , the wave functions in the normal and superconducting regions, taking into account both Andreev and normal reflection processes, can be written as,

$$\begin{aligned} \Psi_N &= \Psi_N^{e+} + r \Psi_N^{e-} + r_A \Psi_N^{h-} \\ \Psi_S &= t \Psi_S^+ + t' \Psi_S^- \end{aligned} \quad (16)$$

where r and r_A are the amplitudes of normal and Andreev reflection respectively, t and t' are the amplitudes of electron-like and holelike quasiparticles in the superconducting region.

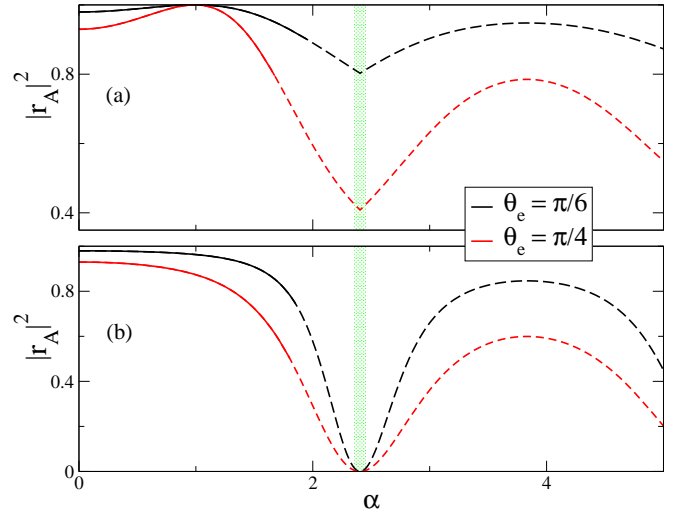


FIG. 1: Plot of $|r_A|^2$ with α for different values of θ_e when the direction of the field is given by (a) $\theta_0 = 0$ and (b) $\theta_0 = \pi/2$. The parameters are set as $\epsilon = 0.02\Delta_0$, $\mu = 100\Delta_0$ and $U_0 = 30\Delta_0$. The shaded/dotted zones denote the regions at and around $J_0(\alpha) = 0$ which are beyond the scope of the present theory.

Here, $k_x^{e(h)} = k_{e(h)}^N \cos \theta$ is the x-component of momentum which is not conserved due to broken translational symmetry, whereas $k_y = k^N \sin \theta$ is conserved. These wave functions must satisfy the boundary condition,

$$\Psi_N(x=0) = \Psi_S(x=0) \quad (17)$$

Using the boundary conditions one can now solve for the coefficients r and r_A to obtain

$$\begin{aligned} r &= \frac{u(e^{i\theta_N^e} - e^{i\theta_S^e}) + v\Gamma(e^{i\theta_N^e} + e^{-i\theta_S^h})}{D}, \\ r_A &= \frac{2 \cos \theta_N^e (v + u\Gamma)}{D}, \\ D &= u(e^{i\theta_S^e} + e^{-i\theta_N^e}) + v\Gamma(e^{-i\theta_N^e} - e^{-i\theta_S^h}), \\ \Gamma &= \frac{v(e^{i\theta_S^e} - e^{-i\theta_N^e})}{u(e^{-i\theta_N^e} + e^{-i\theta_S^h})}. \end{aligned} \quad (18)$$

The differential conductance of the NS junction follows from the Blonder-Tinkham-Klapwijk formula

$$G/G_0 = \int_0^{\pi/2} [1 - |r(\epsilon, \theta, \alpha)|^2 + |r_A(\epsilon, \theta, \alpha)|^2] \times \cos(\theta) d\theta. \quad (19)$$

where G is the conductance across the NS junction and G_0 is the ballistic conductance of metallic graphene⁴¹.

As we see the optical effect to sprout from the anisotropy in the prefactors v_x , v_y (with the ratio being $J_0(\alpha)$), we first probe the effect of the dimensionless optical parameter $\alpha = \frac{2ev_F E_0}{\hbar\omega^2}$ on the andreev/normal reflectance. Fig(1) shows the variation of probability for Andreev reflection ($|r_A|^2$) with α for different values of θ_e . In the regime of $\epsilon < \Delta_0$, no

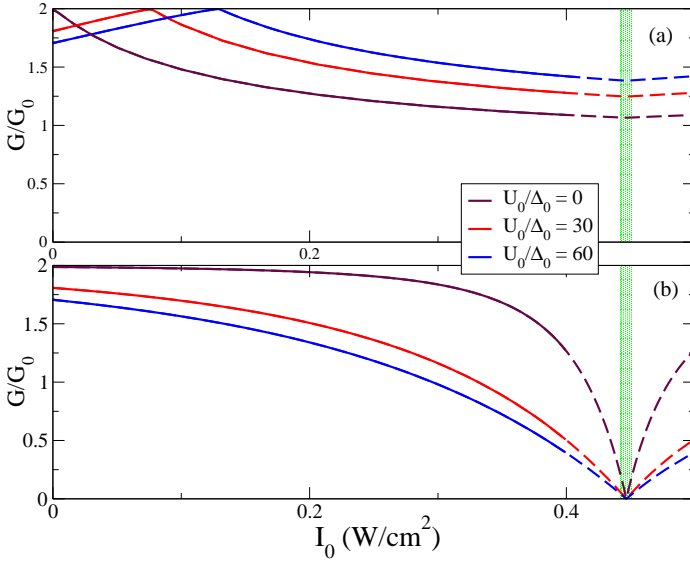


FIG. 2: Plot of differential conductance (G/G_0) of N-S junction versus light intensity I_0 for $U_0 = 0, 30$ and 60 (magenta, purple and pink) respectively with (a) $\theta_0 = 0$ and (b) $\theta_0 = \pi/2$. Here we use $\epsilon = 0.02 \Delta_0$ and $\hbar\omega = 1$ meV. The shaded/dotted regime denotes the zone which are beyond the scope of the present theory. Also the optimally working limit of our theory is the small I_0 limit which is shown schematically by the solid lines (instead of dashed lines that follows).

quasiparticle transport occurs across the NS junction. However, transmission occurs due to Andreev reflection maintaining the constraint $|r|^2 + |r_A|^2 = 1$. In Fig.1(a) we show the variation of $|r_A|^2$ for polarization angle $\theta_0 = 0$ while Fig.1(b) shows the same for $\theta_0 = \pi/2$. The plots are shown for α upto 5 showing the variation of the Andreev reflectance, even though we put our emphasis only on small values (shown by solid lines) of α for which our approximation works the most. In presence of light, the quasiparticles feel additional force along (or opposite to) the electric field direction and accordingly for $\theta_0 = 0$, they bend towards x direction while for $\theta_0 = \pi/2$, they bend towards the y direction. The reduction in the v_y , in the first case, help keeping r_A large due to Klein tunneling while reduction in v_x in the latter case cause r to increase and r_A to diminish (in fact, it causes $r_A = 0$ when v_x vanishes, though this point lies outside the scope of the present theory). In the sub-gap limit, the differential conductance also remains a functional of r_A (or, r) alone. Additionally for $\epsilon < (>)\mu$, retro (specular) type of Andreev reflection develops at the junction². The condition $\mu \gg \Delta_0$ implies $\mu \gg \epsilon$ and retro-reflection is obtained. Note that, we indeed consider this regime of $\epsilon < \Delta_0$ and $\Delta_0 \ll \mu$ in this paper as that is what is achieved comfortably in experiments. However, for the sake of continuity of discussion we also point out that for $\mu \ll \Delta_0$, $\epsilon > \mu$ is obtained only within the restricted range of $\Delta_0 > \epsilon > \mu$ when specular Andreev reflection is observed². As ϵ becomes larger than Δ_0 , normal tunneling begins and Andreev tunneling becomes smaller and smaller.

Let us first discuss shortly the features of the transport phe-

nomena in normal graphene NS junction (i.e., in absence of linearly polarized light or $\alpha = 0$). Without a junction, we will neither have electron reflection nor andreev reflection henceforth yielding $G = G_0$. Now putting a superconductor-interface there witness andreev transport, for $\epsilon < \Delta_0$, thereby increasing the conductivity G . Without any potential barrier (i.e., $U_0 = 0$), G maximizes to $2G_0$ when no electron reflection takes place at the junction. For larger values of ϵ beyond Δ_0 , the electronic system becomes purely resistive and $|r_A|$ gradually decreases down to zero (see Eq.18 for the expressions for r_A). As normal reflection probability increases with barrier height, a larger U_0 results in lesser amount of Andreev reflection and reduced conductivity (see $\alpha = 0$ point in Fig.2). For $\epsilon \gg \Delta_0$, only a small fraction $\sim \Delta_0/\epsilon$ of the incident electrons get Andreev reflected⁴².

Now let us take a look at what a tuning via light irradiation can cause to this transport phenomena. With moderate U_0 , the andreev reflection or r_A is generally large for $\epsilon < \Delta_0$. But with optical irradiation, andreev transport get reduced in a periodic manner, as shown in Fig.1 (for r_A) and Fig.2 (for conductivity). However, for $\theta_0 \rightarrow 0$ and for small α we see an opposite trend in r_A or G . For finite U_0 , it first increases with

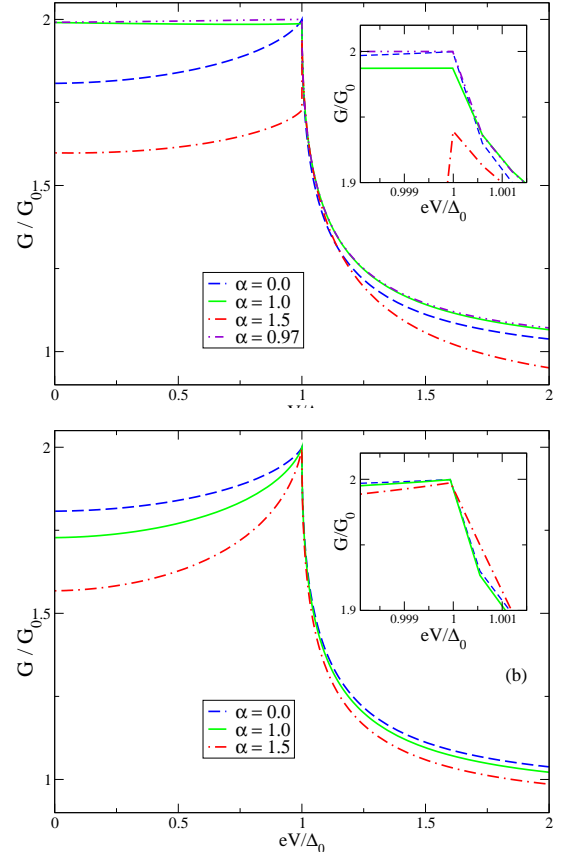


FIG. 3: Plot of differential conductance (G/G_0) of N-S junction as a function of eV/Δ_0 for $\alpha = 0, 1$ and 1.5 (blue, green and red) respectively with (a) $\theta_0 = 0$ and (b) $\theta_0 = \pi/2$. Here we use $U_0 = 30$ and $\Delta_0 = 0.01\mu$. The inset zooms in the region at the conductance peak. Furthermore additional plot at $\alpha = 0.97$ is shown in (a) where complete subgap conductance is observed.

α and start decreasing in an oscillatory fashion only after attaining the maximum at an intermediate α value (see Fig.1(a) and Fig.2(a)). We should point out here that $|r_A|^2$ smoothly goes towards zero for $J_0(\alpha) \rightarrow 0$, as $v_y \rightarrow 0$ in those cases allowing mostly the reflection to happen (only for $U_0 \neq 0$, whereas for $U_0 = 0$, r takes a sharp jump from its minimum to unity where $J_0(\alpha) = 0$). However, this discussion is redundant as our theory breaks down in such limit as many $n' \neq 0$ terms from the summation in Eq. 4 become significant rendering our rotating wave approximation²⁰ type formalism invalid. As discussed for the $\alpha = 0$ case, here also a finite U_0 or Fermi level mismatch results in a reduction in andreev reflection and conductivity. In Fig.2, we have taken the frequency of incident light to be $\hbar\omega=1$ meV and plotted G/G_0 against the light intensity $I_0 = \frac{1}{2}cE_0^2$.

In Fig.3, we show the ϵ dependence of the conductance. With an increase in the excitations above the Fermi level, conductivity increases due to enhanced andreev reflection which becomes maximum at $\epsilon = \Delta_0$. The α dependence that we saw previously in Fig.2 for very small ϵ , survives for larger ϵ ($< \Delta_0$) values as well. At $\epsilon = 0$, conductivity starts from a finite value that is a function of both α and U_0 . As excitation energy increases, so does the Andreev current (for $U_0 \neq 0$) and G/G_0 increases gradually until $\epsilon = \Delta_0$ when the incident quasiparticles no more face any gap at the boundary. Beyond that point G/G_0 show a resistive decay. The critical point $\epsilon = \Delta_0$ also witness a fine reduction in conductance from its maximum value 2 as α becomes nonzero (see the inset in Fig.3). For $\theta_0 = 0$, subgap conductivity remains maximum for one optimum value of α which varies with U_0 (as seen in Fig.2(a)). In fact, the corresponding upturn in conductivity as α is turned on gradually, is responsible for the sudden jump in G/G_0 at/near $\epsilon = \Delta_0$ as seen in Fig.3(a). Mean field condition for superconductivity¹, *i.e.* $\mu + U_0 \gg \Delta_0$ is considered throughout all calculations to ensure that phase coherence is maintained within the S region over a distance of $\lambda_F^S = \frac{\hbar v_F}{\mu + U_0}$.

In the next section, we will discuss about the ABS and Josephson current in an irradiated graphene SNS junction.

IV. ANDREEV BOUND STATES AND JOSEPHSON CURRENT

Josephson supercurrent develops in a SNS junction due to proximity effect³⁴ and this is expressed in terms of the quantized andreev bound states (ABS) developed within the intermediate normal region. To calculate ABS and Josephson current of optically dressed electrons, we consider an irradiated graphene SNS junction where superconducting electrodes are deposited in the left (region-I, with $x < 0$) and right regions (region-II, with $x > L$), leaving a narrow middle region (II) to be the normal graphene (see Fig.4). What we describe below is a brief narrative of graphene SNS junction calculations of Ref.1,41, worked out for our present case incorporating velocity anisotropy. Under exposure to linearly polarized light, the energetics in the three different regions get modified and we construct the wave functions as follows. For $x < 0$, we may

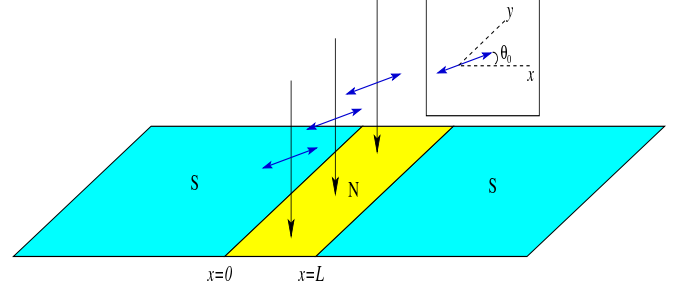


FIG. 4: Light irradiation to a SNS junction with electric field at an angle θ_0 to the x axis (the junction direction in the xy plane).

have,

$$\begin{aligned} \Psi_{S,L} = & t_L^e e^{-iq_e \cos \theta_S^e x} [u(q_e), u(q_e) e^{i(\pi - \theta_S^e)}, v(q_e) e^{-i\phi_L}, \\ & v(q_e) e^{i(\pi - \theta_S^e - \phi_L)}]^T + t_L^h e^{iq_h \cos \theta_S^h x} [v(q_h), \\ & v(q_h) e^{i\theta_S^h}, u(q_h) e^{-i\phi_L}, u(q_h) e^{i(\theta_S^h - \phi_L)}]^T \end{aligned} \quad (20)$$

and for $x > L$,

$$\begin{aligned} \Psi_{S,R} = & t_R^e e^{iq_e \cos \theta_S^e x} [u(q_e), u(q_e) e^{i\theta_S^e}, v(q_e) e^{-i\phi_R}, \\ & v(q_e) e^{i(\theta_S^e - \phi_R)}]^T + t_R^h e^{-iq_h \cos \theta_S^h x} [v(q_h), \\ & v(q_h) e^{i(\pi - \theta_S^h)}, u(q_h) e^{-i\phi_R}, u(q_h) e^{i(\pi - \theta_S^h - \phi_L)}]^T. \end{aligned} \quad (21)$$

In the region $0 \leq x \leq L$, we can construct wave function as given in Eq.(11). Here $\phi_{L,R}$ is the superconducting phase on the left/right side of the normal region, associated with the broken $U(1)$ symmetry in the superconducting state. The macroscopic phase difference is defined as $\phi = \phi_R - \phi_L$. The procedure for calculating the Josephson current is to first obtain the energy spectrum for the Andreev bound states in the intermediate normal region. This is done by matching the wavefunctions at the two NS interfaces, and then solving for the allowed energy states. Explicitly, the boundary conditions dictate that,

$$\Psi_L^S(x=0) = \Psi^N(x=0); \Psi_R^S(x=L) = \Psi^N(x=L) \quad (22)$$

leading to quantization relations between the superconducting phase difference ϕ and the quasiparticle excitation energy ϵ . The boundary conditions in Eq.(22) lead to a matrix equation involving an 8×8 matrix⁷

$$\mathcal{M} = \begin{pmatrix} \mathcal{M}_{11} & \mathcal{M}_{12} \\ \mathcal{M}_{21} & \mathcal{M}_{22} \end{pmatrix} \quad (23)$$

for transmission and reflection coefficients and the non-trivial solutions exist for $\det(\mathcal{M}) = 0$. The 4×4 matrices \mathcal{M}_{ij} are explicitly given in appendix. In order to proceed with the analytical solution we assume the superconducting regions to be heavily doped, *i.e.*, $\mu_s \gg \mu$ (here $\mu_s = \mu + U_0$, is the effective chemical potential within the S regions). In this case, $\theta_S^e = \theta_S^h = \delta$ and the number of propagating modes in superconducting region becomes $N = \mu_s W / \pi \hbar v_F$ where W

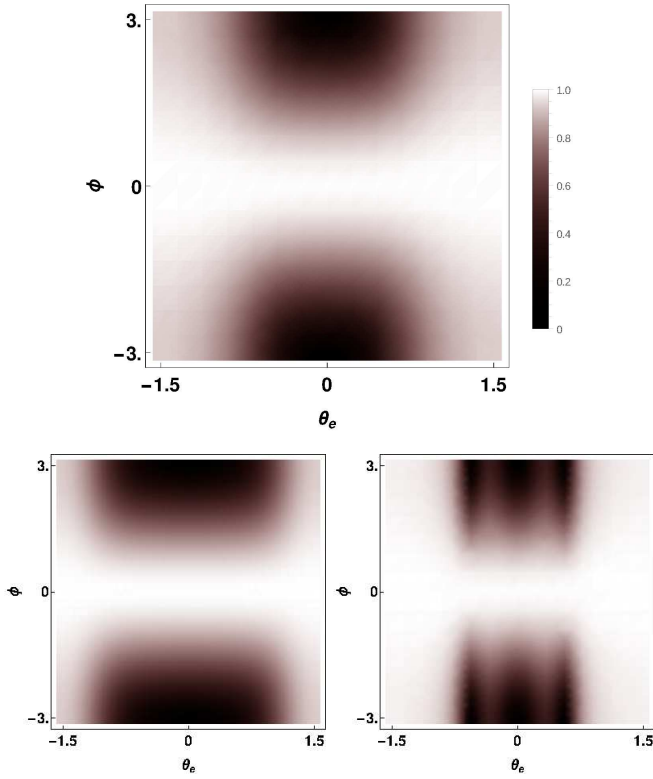


FIG. 5: Plot of ABS in the Josephson S|N|S junction with ϕ and θ_e in (top) absence and (bottom) presence of a dressing field with $\alpha = 1.5$. We have set $\mu L/\hbar v_F = 2.5$. The field directions are considered to be along x (bottom-left) and y (bottom-right) respectively.

denotes the width of the N region with $W \gg L$. In the regime of "short-junction" limit ($\Delta_0 L/\hbar v_F \ll 1$) and heavily doped superconductor, one can effectively put $\delta \rightarrow 0$. Within the approximations, the quantized states are obtained in terms of θ and μ of the N region. The expression is obtained as,

$$\epsilon_n(\phi) = \Delta_0 \sqrt{1 - \gamma_n \sin^2 \phi/2} \quad (24)$$

where γ_n is the transmission probability through the middle region and is obtained as,

$$\gamma_n = \frac{k_x^2}{k_x^2 \cos^2(k_x L) + \frac{\mu^2}{\hbar^2 v_F^2} \sin^2(k_x L)}$$

$$k_x L = \sqrt{\left(\frac{\mu L}{\hbar v_F}\right)^2 - J_0^2(\alpha) q_n^2 L^2} \quad (25)$$

Here k_x and q_n denote the wave-vectors along x and y directions respectively where the transverse wavevectors, for infinite mass confinement⁴³, are quantized as $q_n = (n + \frac{1}{2})\pi/W$. The resonant electron-hole states represented by these $\epsilon_n(\phi)$ are called the andreev bound states (for $|\epsilon_n(\phi)| < \Delta_0$). Note that for $\alpha = 0$, Eq.(25) is reduced to the form as given in Ref.36. The Andreev modes collectively contribute to the

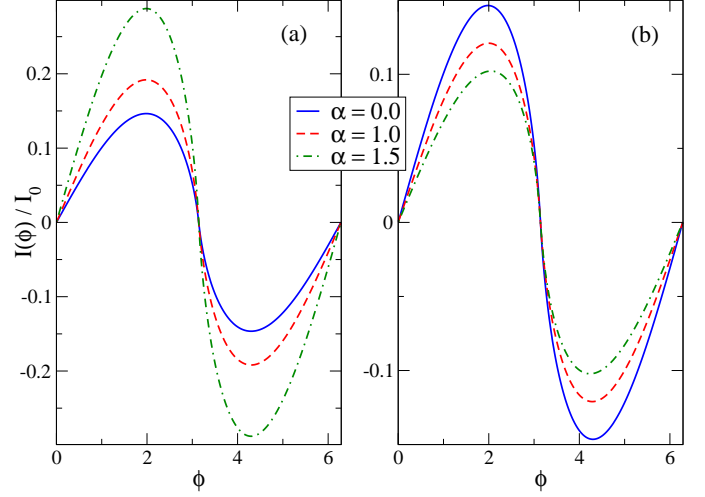


FIG. 6: Plot of Josephson current $I(\phi)/I_0$ as a function of ϕ with α as a parameter corresponding to the electric field of light along (a) x -direction and (b) y -direction respectively. In both the plots we set $\mu L/\hbar v_F = 1$, $W/\xi = 30$, $\mu_s/\Delta_0 = 150$ and $L/\xi = 0.1$.

Josephson supercurrent as³⁶,

$$I(\phi) = \frac{e\Delta_0}{\hbar} \sum_n \gamma_n \sin \phi / \epsilon_n(\phi) \quad (26)$$

In short junction limit, we may replace the summation in Eq.(26) over the quantized modes with an integration: $\sum_n \rightarrow \frac{W}{2\pi} \int dq_n$.

Now we observe how ABS depends on the optical parameter α . Fig.5 shows the comparison between $\alpha = 0$ and $\alpha = 1.5$. Without irradiation, electrons incident normally (*i.e.*, $\theta_e = 0$) causes the bound-state energy to become zero at $\phi = (-\pi, \pi)$, whereas $\epsilon_n(\phi) = \Delta_0$ (*i.e.*, andreev modes remains bound no more) when $\theta_e \rightarrow \pm\pi/2$. With the dressing field, such angular dependence of zero-ABS regime - which contributes most to the superconduction, spread more for $\theta_0 = 0$ or become an oscillating pattern for $\theta_0 = \pi/2$ (where further null values are obtained at discrete oblique incident angles when $\gamma_n \rightarrow 1$). These can be seen in Fig.5 bottom panels.

Experimentally, ABS features can also be perceived by noticing the current phase relation which is shown in Fig.6. The Josephson current is sensitive to the direction of light irradiation on the graphene. This is due to fact that the transmission probability γ_n is enhanced or suppressed when light radiation is along x or y -direction respectively.

The behavior of critical current I_c of irradiated graphene-based Josephson junction vs $\mu L/\hbar v_F$ is shown in Fig.7. Fig.7(a) shows the plot of I_c/I_0 ($I_0 = e\Delta_0/\hbar$) for the light irradiation is along x -direction. As shown, the value of I_c of irradiated graphene becomes larger with finite α as compared to its normal value (for $\alpha = 0$) at the charge neutrality point. This is an interesting observation given the fact that graphene transport is already special due to nonzero Josephson current at $\mu = 0$ notwithstanding its zero DOS, first shown analytically by Titov and Beenakker (Ref.36). When light is irradi-

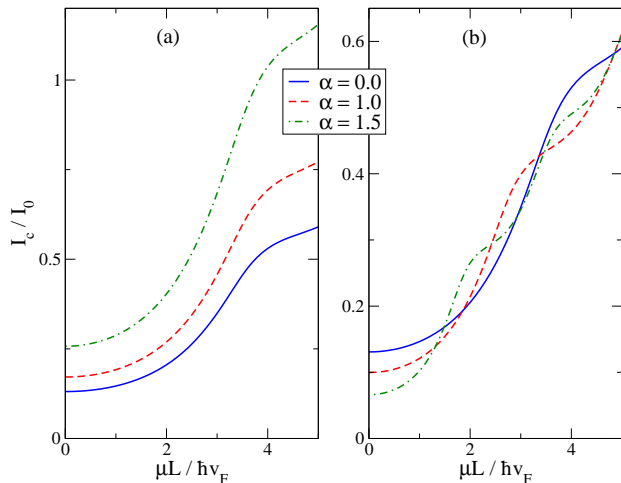


FIG. 7: Plot of critical current (I_c/I_0) with $\frac{\mu L}{\hbar v_F}$ with α as a parameter for (a) $\theta_0 = 0$ and (b) $\theta_0 = \pi/2$. Both the plots correspond to $W/\xi = 30$, $\mu_s/\Delta_0 = 150$ and $L/\xi = 0.1$.

ated along y-direction the expression of γ_n and k_x in Eq.25 is modified as,

$$\gamma_n = \frac{J_0^2(\alpha)k_x^2}{J_0^2(\alpha)k_x^2 \cos^2(k_x L) + \frac{\mu^2}{\hbar^2 v_F^2} \sin^2(k_x L)}$$

$$k_x L = \frac{\sqrt{(\frac{\mu L}{\hbar v_F})^2 - q_n^2 L^2}}{J_0(\alpha)} \quad (27)$$

The value of I_c with $\mu L/\hbar v_F$ is shown in Fig.7(b). It shows that, I_c decreases with α at $\mu \rightarrow 0$. For nonzero μ , however, the value of I_c and hence Josephson current of irradiated graphene can be either enhanced or suppressed depending on the values of μ and α used. All these behavior can be understood examining the expression for γ_n in Eq.(25) and Eq.(27). For $\mu = 0$, all the transport modes n become evanescent and γ_n decays slower and faster as a function of q_n in Eq.(25) and Eq.(27) respectively. These results, to some extent, resemble that from a strained monolayer graphene, as detailed in Ref.[7,44]. There, an applied mechanical strain on a monolayer graphene breaks the isotropy in the velocity of a quasiparticle by modifying the hopping parameter and thereby makes the low energy spectrum anisotropic. This route, therefore, leads to similar outcome as ours. However, since a light-controlled electronic device is typically much faster and easily controllable than those mechanically or electrically controlled devices, an optical tuning stands out as a more feasible means to the experimentalists and we believe that our findings can encourage a lot during building of future spintronic devices.

V. CONCLUSION

In summary, we have studied extensively the Andreev transport and Josephson effect in light irradiated, proximity in-

duced graphene NS and narrow SNS junctions. In the off-resonant condition that we study, the resulting Dirac spectrum becomes anisotropic which unravels many unusual phenomena such as reduction/enhancement of the subgap conductance as well as the Josephson currents, depending on the direction of polarization. In one extreme, we can tune in maximum andreev conductivity in presence of Fermi level mismatch, for irradiated field along the junction direction. On the other hand, noticeable reduction in AR is possible when the polarization points parallel to the interface/junction. This latter feature can be utilized in getting enhanced crossed Andreev reflection⁴⁵ (CAR) in an irradiated graphene based NSN junction. Usually in graphene NSN junctions, CAR is not perceived much due to the local AR and elastic co-tunneling (EC) processes, unless raising and lowering of the chemical potentials are performed considering nSp or pSn type graphene bipolar transistors⁴⁶. However, in an irradiated graphene sheet, AR can be tuned to get considerably suppressed. So it will be interesting to investigate the optical effect in strengthening the CAR signal even without shifting the chemical potential of the normal leads and thereby causing the non-local cooper pair splitting that spatially separates the entangled electron pairs⁴⁷. In fact, such investigation will comprise our future plan of work. Lastly, irradiation causes redistribution of the low energy regime in the Andreev bound state. And as we have seen, it can be tuned properly to produce enhanced supercurrent through a graphene based SNS junction, even at the Dirac point in the spectrum.

These interesting observations, in fact, can provide possible route to control quantum transport in graphene with relevance to the spintronic based applications. It will be equally interesting to see the effect of light irradiation in transition metal dichalcogenides such as silicene⁴⁸ or MoS_2 ⁴⁹ where spin orbit interaction plays an important role in transport.

VI. ACKNOWLEDGMENTS

The authors thank K. Sengupta for useful discussions. SK acknowledges financial support from CSIR, India, under Scientists' Pool Scheme No. 13(8764-A)/2015-Pool.

VII. APPENDIX

Here, we give the matrix form of \mathcal{M}_{ij} in Eq.(23) of the main text. The matrix form can be easily constructed by matching the wave function in two NS regions and ABS is obtained from the nontrivial solution of the eigenvalue equation $\mathcal{M}x = 0$. Using Eq.(11), Eq.(20) and Eq.(21), the matrix forms are obtained as,

$$\begin{aligned}
\mathcal{M}_{11} &= \begin{pmatrix} u(q_e) & v(q_h) & -1 & -1 \\ u(q_e)e^{i(\pi-\theta_e)} & v(q_h)e^{i\theta_h} & -e^{i\theta} & e^{-i\theta} \\ v(q_e)e^{-i\phi_L} & u(q_h)e^{-i\phi_L} & 0 & 0 \\ v(q_e)e^{i(\pi-\theta_e-\phi_L)} & u(q_h)e^{i(\theta_h-\phi_L)} & 0 & 0 \end{pmatrix} & \mathcal{M}_{12} &= \begin{pmatrix} 0 & 0 & 0 & 0 \\ 0 & 0 & 0 & 0 \\ -1 & -1 & 0 & 0 \\ e^{i\theta_A} & -e^{-i\theta_A} & 0 & 0 \end{pmatrix} \\
\mathcal{M}_{21} &= \begin{pmatrix} 0 & 0 & -e^{ik_e \cos \theta x} & -e^{-ik_e \cos \theta x} \\ 0 & 0 & -e^{i\theta} e^{ik_e \cos \theta x} & e^{-i\theta} e^{-ik_e \cos \theta x} \\ 0 & 0 & 0 & 0 \\ 0 & 0 & 0 & 0 \end{pmatrix} \\
\mathcal{M}_{22} &= \begin{pmatrix} 0 & 0 & u(q_e)e^{iq_e \cos \theta_e L} & v(q_h)e^{-iq_h \cos \theta_h L} \\ 0 & 0 & u(q_e)e^{iq_e \cos \theta_e L} e^{i\theta_e} & v(q_h)e^{i(\pi-\theta_h)} e^{-iq_h \cos \theta_h L} \\ -e^{ik_h \cos \theta_A x} & -e^{-ik_h \cos \theta_A x} & v(q_e)e^{-i\phi_R} e^{iq_e \cos \theta_e L} & u(q_h)e^{-iq_h \cos \theta_h L} e^{-i\phi_R} \\ e^{i\theta_A} e^{ik_h \cos \theta_A x} & -e^{-i\theta_A} e^{-ik_h \cos \theta_A x} & v(q_e)e^{-i(\theta_e-\phi_R)} e^{iq_e \cos \theta_e L} & u(q_h)e^{-iq_h \cos \theta_h L} e^{i(\pi-\theta_h-\phi_R)} \end{pmatrix} \quad (28)
\end{aligned}$$

-
- ¹ C. W. J. Beenakker, Phys. Rev. Lett. 97, 067007 (2006).
² C. W. J. Beenakker, Rev. Mod. Phys. 80, 1337 (2008).
³ A. H. C. Neto *et al.*, Rev. Mod. Phys. 81, 109 (2009).
⁴ S. D. Sharma *et al.*, Rev. Mod. Phys. 83, 407 (2011).
⁵ K. S. Novoselov, A. K. Geim, S. V. Morozov, D. Jiang, Y. Zhang, S. V. Dubonos, I. V. Grigorieva, A. A. Firsov, Science 306 (5696), pp. 666669 (2004).
⁶ R. C-Bastos, C. Leon, D. Faria, A. Latge, E. Y. Andrei, N. Sandler, Phys. Rev. B 94, 125422 (2016).
⁷ M. Alidoust, J. Linder, Phys. Rev. B 84, 035407 (2011).
⁸ L. Majidi, M. Zareyan, Phys. Rev. B 86, 075443 (2012).
⁹ M. Farhat, S. Guenneau, H. Bagci, Phys. Rev. Lett. 111, 237404 (2013).
¹⁰ J. Schiefele, J. Pedros, F. Sols, F. Calle, F. Guinea, Phys. Rev. Lett. 111, 237405 (2013).
¹¹ S. Xiao, X. Zhu, B.-H. Li, N. A. Mortensen, Front. Phys. 11(2), 117801 (2016).
¹² I. V. Iorsh, I. S. Mukhin, I. V. Shadrivov, P. A. Belov, Y. S. Kivshar Phys. Rev. B 87, 075416 (2013).
¹³ O. V. Kibis, S. Morina, K. Dini and I. A. Shelykh, A.Phys.Pol.A 127, 528(2016).
¹⁴ A. Furio *et al.*, Nanotechnology, 28, 054003 (2017).
¹⁵ O. V. Kibis, S. Morina, K. Dini and I. A. Shelykh, Phys. Rev. B, 93, 115420 (2016).
¹⁶ K. Kristinsson, O. V. Kibis and I. A. Shelykh, Sci. Report, 6, 20082 (2016);
¹⁷ D. Yudin, O. V. Kibis and I. A. Shelykh, NJP 18, 103014 (2016)
¹⁸ O. V. Kibis, K. Dini, I. V. Iorsh and I. A. Shelykh, Phys. Rev. B, 95 125401 (2017)
¹⁹ D. Yudin, I. A. Shelykh, Phys. Rev. B 94, 161404 (R) (2016)
²⁰ S. Ashhab *et al.*, Phys. Rev. A75, 063414 (2007).
²¹ X. Zhou, G. Jin, Phys. Rev. B 94, 165436 (2016).
²² H. L. Calvo, H. M. Pastawski, S. Roche and L. E. F. Torres, Applied. Phys. Lett 98, 232103 (2011)
²³ G. Usaj, P. M. Perez-Piskunow, L. E. F. Torres and C. A. Balseiro, Phys. Rev. B 90, 115423 (2014)
²⁴ X. Zhou, Y. Xu and G. Jin, Phys. Rev. B 92, 235436 (2015)
²⁵ O. V. Kibis, Phys. Rev. B 86, 155108 (2012)
²⁶ S. Morina, O. V. Kibis, A. A. Pervishko, I. A. Shelykh, Phys. Rev. B 91, 155312 (2015)
²⁷ A. A. Pervishko, O. V. Kibis, S. Morina, I. A. Shelykh, Phys. Rev. B 92, 205403 (2015)
²⁸ O. V. Kibis, Phys. Rev. Lett. 107, 106802 (2011)
²⁹ H. Hübener *et al.*, Nature Communication 8, 13940 (2017)
³⁰ D. Sinha, Eur. Phys. Lett. 115, no. 3, 37003 (2016).
³¹ X. Zhai and G. Jin, Phys. Rev. B 89, 235416 (2014).
³² M. Ezawa, Phys. Rev. Lett 100, 026603 (2013)
³³ T. Kitagawa, T. Oka, A. Brataas, L. Fu, and E. Demler, Phys. Rev. B 84, 235108 (2011)
³⁴ Heersche, H. B., P. Jarillo-Herrero, J. B. Oostinga, L. M. K. Vandersypen, and A. Morpurgo, 2007, Nature 446, 56.
³⁵ J. Linder, A. Sudbo, Phys. Rev. B 77, 064507 (2008).
³⁶ M. Titov, C. W. J. Beenakker, Phys. Rev. B74, 041402 (2006).
³⁷ M. Maiti, K. Sengupta, Phys. Rev. B76, 054513 (2007).
³⁸ J. Linder *et al.* Phys. Rev. B 80, 094522 (2009)
³⁹ S. V. Syzranov, Ya. I. Rodionov, K. I. Kugel and F. Nori, Phys. Rev. B 88, 241112 (2013)
⁴⁰ M. I. Katsnelson, K. S. Novoselov, and A. K. Geim, Nat. Phys. 384, 620 (2006).
⁴¹ S. Bhattacharjee, K. Sengupta, Phys. Rev. Lett. 97, 217001 (2006).
⁴² G. E. Blonder, M. Tinkham, Phys. Rev. B27, 112 (1983).
⁴³ J. Tworzydło *et al.*, Phys. Rev. Lett. 96, 246802 (2006).
⁴⁴ Y. Wang, Y. Liu and B. Wang, Appl. Phys. Lett. 103, 182603 (2013)
⁴⁵ G. Deutscher, Jour. of Sup., vol 15, no.1, page 43 (2002)
⁴⁶ J. Csýssol, Phys. Rev. Lett. 100, 147001 (2008).
⁴⁷ Y. S. Ang, L. K. Ang, C. Zhang, and Z. Ma, Phys. Rev. B93, 041422(R) (2016)
⁴⁸ X. Zhou, and G. Jin, Phys. Rev. B94, 165436 (2016).
⁴⁹ A. T. Neal, H. Liu, J. Gu, and P. D. Ye, ACS Nano 7(8), pp 7077 (2013).